Polymer Testing 154 (2026) 109056

Contents lists available at ScienceDirect

Polymer Testing

journal homepage: www.elsevier.com/locate/polytest

Efficient adsorption of iodine by three-dimensional organic polymers synthesized by single step substitution and mechanism study

Fei-Fei Wang [a], Qing-Rong Zhang [a], Chang Liu [b,*], Qian Zhang [a], Guangyao Hou [c], Rui Zhang [d,**]

[a] Department of Chemistry, Xinzhou Normal University, Xinzhou, 034000, PR China
[b] College of Criminal Science and Technology (College of Forensic Science), Criminal Investigation Police University of China, Shenyang, 100854, PR China
[c] School of Materials Science and Engineering, Harbin Institute of Technology, Harbin, Heilongjiang, 150001, PR China
[d] Shenyang Key Laboratory of Medical Molecular Theranostic Probes in School of Pharmacy, School of Pharmacy, Shenyang Medical College, Shenyang, 110034, PR China

ARTICLE INFO

Keywords:
Three-dimensional organic polymer
Iodine adsorption
DFT calculation
Adsorption mechanism

ABSTRACT

In this paper, we report the preparation of a novel three-dimensional organic polymer synthesized via a one-step substitution reaction utilizing dl-dithiothreitol and 2,4,6-tribromomethyltrimethylbenzene as raw materials. This polymer features a straightforward preparation process, low synthesis cost, and potential for large-scale production. The structural characterization of the polymer was conducted using various techniques, including solid-state carbon-13 nuclear magnetic resonance (^{13}C NMR), infrared spectroscopy (IR), thermogravimetric analysis (TGA), and powder X-ray diffraction (PXRD). Building on its structural characteristics, we further investigated the polymer's adsorption capacity for both gaseous iodine and iodine in aqueous solutions. Experimental results confirm that the polymer exhibits efficient and selective iodine adsorption with no structural alteration before and after the capture process. The maximum adsorption capacity for iodine vapor reached 4.60 g g^{-1}. For aqueous solutions with concentrations of 0.12 mmol L^{-1} and 0.30 mmol L^{-1}, the maximum adsorption capacities were determined to be 6.25 mg g^{-1} and 24.58 mg g^{-1}, respectively.

Extensive density functional theory (DFT) calculations revealed that multiple noncovalent interactions, including I−I···π, C−H···I, and O−H···I bonding, as well as electrostatic interactions between the polymer and I_2/I_3^- species, collectively account for its exceptional iodine trapping capacity.

1. Introduction

Driven by the increasing global energy demand and the pursuit of carbon neutrality, the limitations and environmental impacts of traditional fossil fuels have become increasingly evident [1–3]. Nuclear energy, characterized by its high energy density and low carbon emissions, has emerged as a crucial option for addressing the global energy crisis and combating climate change [4,5]. However, during nuclear fission processes, radioactive isotopes such as ^{129}I and ^{131}I are generated [6,7]. In the event of a nuclear accident, these radioactive elements may leak into the environment in gaseous, liquid, or solid forms, posing significant risks to both ecological systems and human health with far-reaching and long-lasting consequences [8–10]. The gaseous and liquid I_2 can cause damage to the ecological environment, such as radiation damage, air pollution and climate change [11,12]. Therefore, the development of effective I_2 capture methods has recently aroused strong interest.

Adsorption method has the advantages of simple operation, good environmental sustainability and strong stability, and has become one of the most effective methods for iodine capture [13]. Over the past few decades, various materials for adsorbing iodine have been studied. Such as covalent organic framework materials (COFs) [14], calixarene [15], silica [16], activated carbon [17], zeolite [18], covalent organic porous polymers (POPs) [19], metal-organic framework materials (MOFs) [20], metal-organic polyhedral materials (MOPs) [21], and so on. Among them, porous zeolite materials have high stability and renewability, making them one of the most commonly used adsorbents for wastewater treatment [22]. However, due to its relatively slow adsorption rate and limited adsorption capacity for certain substances, its wide application in nuclear waste treatment is restricted. MOFs are also applied in iodine

* Corresponding author.
** Corresponding author.
E-mail addresses: 2024990017@cipuc.edu.cn (C. Liu), ruizhang@symc.edu.cn (R. Zhang).

https://doi.org/10.1016/j.polymertesting.2025.109056
Received 16 September 2025; Received in revised form 8 November 2025; Accepted 23 November 2025
Available online 26 November 2025

capture [23]. They have the characteristics of high porosity, diverse surface functions and large specific surface area [24]. Nevertheless, in view of their low yield and high price, they still pose challenges in the commercial application of iodine capture and treatment. COFs exhibit excellent thermal stability, enabling efficient iodine capture at high temperatures and in solution environments [25]. These materials hold significant practical potential for addressing emergency releases of radioactive or organic iodine during nuclear accidents. However, their application is limited by relatively low removal efficiency. Therefore, there is an urgent need to develop new materials for capturing gaseous iodine and iodine in aqueous solutions. In particular, this material has the advantages of simple preparation, excellent stability and low synthesis cost.

Organic polymer materials offer several advantages, including straightforward synthesis, cost-effectiveness, and the potential for large-scale production [26]. To date, various organic polymer materials have been developed for the removal of persistent organic pollutants [27]. Similarly, these materials demonstrate superior adsorption capacity for iodine and have attracted increasing attention in the recent research. Cao et al. designed and synthesized a pillar [5]arene based three-dimensional polymer network for iodine capture from water [28]. It has a high adsorption efficiency and can remove over 90 % of iodine within 30 min of shaking. Wang et al. developed a β-cyclodextrin-based porous amorphous material CDPN with excellent gas-phase iodine capture performance [29]. The strong interaction between the host (CDPN) and the guest (I_2) was promoted by using cyclodextrin cavities and cross-linked polymer networks, and the iodine absorption capacity of CDPN was 2.73 g g^{-1}. More studies on the adsorption of iodine by organic polymers are provided in Table S1. However, to date, the majority of research on organic polymers has concentrated on the adsorption of iodine in aqueous solutions or gaseous iodine within a singular environment. Few studies have explored the simultaneous application of organic polymers for iodine capture in both gaseous and solution-based environments.

In this paper, a new type of three-dimensional organic polymer (**DTTB3**) was prepared by one-step substitution utilizing dl-dithiothreitol and 2,4,6-tribromomethyltrimethylbenzene as raw materials. The hydroxyl groups (−OH) inherent in dl-dithiothreitol serve as the core adsorption sites for iodine. Meanwhile, the three bromomethyl groups ($-CH_2Br$) in 2,4,6-tribromomethyltrimethylbenzene function as highly reactive moieties. These bromomethyl groups can undergo substitution reactions with the sulfhydryl groups (−SH) of dl-dithiothreitol, which facilitates the efficient construction of a three-dimensional (3D) polymeric network. By exploring the adsorption performance of **DTTB3** for iodine vapor and iodine solution, demonstrates superior iodine adsorption capacity and reusability. Impressively, **DTTB3** achieves a record-high iodine uptake of 4.60 g g^{-1} from iodine vapor, and exhibits over 90 % removal efficiencies of iodine during iodide ion capture experiments in an aqueous solution, which is more than twice that of commercial activated carbon materials. Furthermore, the pore architecture and thermal stability of polymeric materials serve as pivotal guarantees for the efficient adsorption of iodine in nuclear wastewater. Extensive density functional theory (DFT) calculations demonstrated that multiple noncovalent interactions, including I−I···π, C−H···I, O−H···I bonds, and electrostatic interactions between **DTTB3** and I_2/I_3^-, which contribute the high iodine trapping capacity.

2. Experiments

2.1. Materials and instruments

2,4,6-tribromomethyltrimethylbenzene, dl-dithiothreitol, K_2CO_3, and KCl were purchased from Aladdin. Acetonitrile and hydrochloric acid (*wt.* 38 %) were obtained from Yangzhou Huafu Chemical Co., LTD. I_2 were purchased from Tianjin Fengchuan Chemical Reagent Co., LTD. All chemicals are analytical reagent grade and can be used directly without further purification. The instrument and parameter descriptions related to this experiment are provided in the Supporting *Information*.

2.2. Synthesis of DTTB3

Firstly, dl-dithiothreitol (0.75 g, 4.80 mmol) and 2,4,6-tribromomethyltrimethylbenzene (0.48 g, 1.20 mmol) were introduced into a 50 mL three-necked flask, followed by the addition of 25 mL of acetonitrile as the solvent. Then, the mixture was stirred at room temperature for 30 min before adding K_2CO_3 (1.50 g, 10.80 mmol). Subsequently, the reaction was continued under stirring at a temperature of 70 °C for 72 h in a nitrogen atmosphere. The product was filtered by vacuum filtration, and washed successively with acetonitrile, dilute hydrochloric acid, distilled water and acetonitrile, and then naturally dried at room temperature. Finally, the product was obtained with a yield of 95.30 % (calculated based on 2,4,6-tribromomethyltrimethylbenzene). The synthesis process of the polymer is shown in Scheme 1.

2.3. Adsorption and release of iodine vapor

Take **DTTB3** (50 mg) and elemental iodine (900 mg) in 10 mL small beaker, respectively. Subsequently, place the two small beakers together in a sealed wide-mouthed bottle, and then put the wide-mouthed bottle into an oven at 75 °C (simulating the reprocessing temperature of nuclear fuel). Take out the breaker of **DTTB3** after time intervals of 0.5, 1, 2, 3, 4, 6, 8 and 12 h, respectively, and weigh them after cooling to room temperature. Calculate the adsorption capacity of iodine based on the increase in the mass of **DTTB3**. During the release process, the adsorbed **DTTB3** is soaked and rinsed with methanol until the solution is colorless.

2.4. Adsorption of iodine in aqueous solution

Prepare 100 mL of I_3^- (0.3 mM, [KI]/[I_2] = 3/1) solution, and perform gradient dilution to obtain six sets of iodine standard solutions with concentrations of 0.27, 0.24, 0.21, 0.18, 0.15, and 0.12 mM, respectively. These solutions should be stored in a dark environment for future use. Take a 0.12 mM iodine solution (3 mL) into a cuvette and add 5 mg of **DTTB3** to it, and mix thoroughly. At different time intervals, the absorbance was measured by an ultraviolet–visible (UV–Vis) spectrophotometer. The removal rate (E, %) and adsorption capacity (q_e, mg/g) of iodine were calculated according to eq (1) and eq (2),

$$E = (C_0 - C_e) / C_0 \times 100\% \quad (1)$$

$$q_e = (C_0 - C_e) / m \times V \quad (2)$$

where C_0 and C_e represent the initial concentration (mg mL^{-1}) and the remaining concentration (mg mL^{-1}) of iodine, respectively, m and V stand for the mass of **DTTB3** (mg) and the volume of the iodine solution (mL), respectively. All experiments were conducted in pure water.

3. Results and discussion

3.1. Structural characterization

Fig. 1a and b presents the scanning electron microscope (SEM) images of the synthesized **DTTB3**. These images reveal that **DTTB3** consists of amorphous particles with irregular shapes and sizes, exhibiting a loose and porous structure. Furthermore, to investigate the structure of the 3D organic polymer, ^{13}C CP-MAS NMR was using to characterized **DTTB3** (Fig. 1c). A peak centered at δ 12 ppm was assigned to the carbon atoms of the methyl group on the benzene ring. The signals between 124 and 135 ppm corresponded to two types of carbon atoms on the benzene of the polymer, and the two sets of peaks between 20 and 56 ppm correspond to two types of carbon atoms connected with sulfur atoms, which proves the successful synthesis of **DTTB3**. Meanwhile, the peak

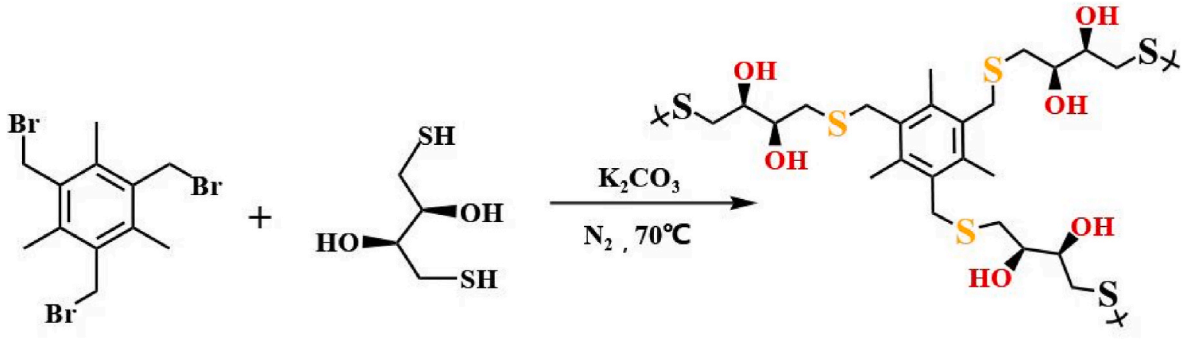

Scheme 1. Schematic illustration of the synthesis process of **DTTB3**.

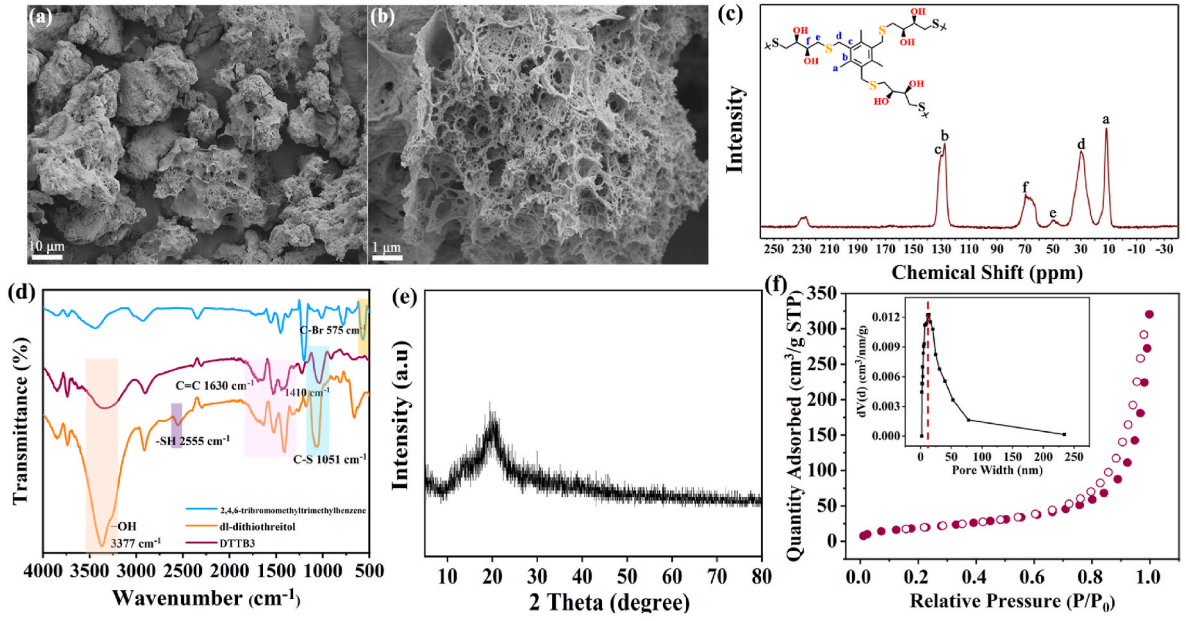

Fig. 1. SEM images (a, b), ^{13}C NMR spectrum (c), FT-IR spectrum (d), PXRD pattern (e), N_2 adsorption-desorption isotherm and pore size distribution curve (f) of **DTTB3**.

centered at δ 228 ppm was regarded as carbonyl carbon due to the dehydration condensation of hydroxyl groups in the polymer. Fig. 3d presents the FT-IR spectra of 2,4,6-tribromomethyltrimethylbenzene, dl-dithiothreitol, and **DTTB3**, respectively. The spectrum of **DTTB3** reveals an absorption peak at 1051 cm^{-1}, which can be attributed to the presence of C–S groups [30]. Additionally, two prominent absorption peaks were observed at 1630 and 1410 cm^{-1}, corresponding to the stretching vibration of the C=C skeleton in the benzene ring structure of **DTTB3** [31]. The peak located at 3377 cm^{-1} is associated with –OH groups present in both **DTTB3** and dl-dithiothreitol [32]. Furthermore, the characteristic peak of –SH at 2555 cm^{-1} in dl-dithiothreitol and the C–Br stretching peak at 575 cm^{-1} in 2,4,6-tribromomethyltrimethylbenzene both disappeared, indicating successful reaction between the two monomers and the formation of the polymer **DTTB3** [33,34]. Fig. 3e illustrates the PXRD pattern of **DTTB3**. An analysis of this figure reveals prominent broad peak around 20°. This peak broadening may be attributed to varying degrees of local order within the structure of **DTTB3** [35], resulting in diffuse diffraction peaks and suggesting that **DTTB3** exhibits characteristics typical of an inhomogeneous amorphous material [36]. To further investigate the specific surface area and pore structure of **DTTB3**, a nitrogen adsorption-desorption isotherm was performed at 77K. As illustrated in Fig. 3f and its inset, the initial behavior in the low-pressure region ($P/P_0 < 0.4$) shows that the adsorption and desorption curves basically overlapping. As the relative pressure increases into the mid-pressure range ($0.4 < P/P_0 < 0.8$), a modest increase in nitrogen uptake is observed. At high-pressure condition ($P/P_0 > 0.8$), there is a pronounced increase in the amount adsorbed. This observation indicates that the isotherm exhibits characteristics of both type II and type IV behaviors [37]. Notably, a small H3 hysteresis loop is present within the isotherm [38], suggesting that **DTTB3** predominantly possesses mesoporous properties. Utilizing the density functional theory (DFT) method, it was determined that the average pore size of **DTTB3** is 13.40 nm, with a specific surface area of 72.19 $m^2\ g^{-1}$. During the iodine adsorption process, iodine molecules (with a molecular diameter of approximately 0.49 nm) must first diffuse into the polymer pores before being retained *via* surface interactions. The pore volume of **DTTB3** reaches 0.45 cm^3/g, significantly exceeding that of conventional polymers with low pore volumes, indicating the presence of abundant internal cavity structures. The thermogravimetric analysis (TA) of **DTTB3** was conducted in a nitrogen atmosphere over a temperature range from 0 °C to 1000 °C (Fig. S1). **DTTB3** remains relatively stable up to 150 °C. Within the temperature range of 150 °C–345 °C, **DTTB3** undergoes a weight loss of approximately 75 %. The thermal stability of polymeric materials is a critical property for their application in iodine vapor adsorption during nuclear fuel reprocessing, as well as in iodine species adsorption from nuclear wastewater.

3.2. Iodine vapor adsorption

Iodine vapor adsorption research was initially conducted to assess the iodine adsorption properties of **DTTB3**. The polymers were exposed to an iodine vapor atmosphere at 75 °C under atmospheric pressure, simulating conditions akin to nuclear fuel reprocessing. As illustrated in Fig. 2a, the adsorption capacity of **DTTB3** for iodine vapor increases continuously over time. The iodine vapor adsorption curve indicates that the initial adsorption rate is relatively rapid during the first 10.5 h, achieving an adsorption capacity of 3.91 g g^{-1}, which constitutes approximately 85 % of total uptake. After a duration of 24.5 h, there was negligible change in polymers weight, and the polymers' iodine vapor adsorption capacity reached 4.56 g g^{-1}. The adsorption process was completed after 36.5 h, and the maximum adsorption capacity of iodine vapor reached 4.60 g g^{-1}. To gain a comprehensive understanding of the adsorption process, two well-established kinetic models were employed for data simulation (Fig. 2b). A comparison of the fitting results reveals that the experimental kinetic data exhibit a significantly better fit to the pseudo-first-order model than to the pseudo-second-order model [39, 40]. This observation obviously reveals that physical was the predominant mechanism governing the adsorption process. Subsequently, to evaluate the recyclability of **DTTB3** to adsorb iodine vapor, five cycles of adsorption experiments were conducted (Fig. 2c). It was observed that after five cycles, the adsorption capacity for iodine decreased from 3.91 g g^{-1} in the first cycle to 3.45 g g^{-1} in subsequent round, representing a reduction of approximately 11.76 %. This indicates that **DTTB3** exhibits good recyclability in adsorption of iodine vapor. Upon reaching equilibrium, a noticeable color change occurred to **DTTB3**, transitioning from light yellow to dark black (Fig. 2d–f), signifying that **DTTB3** had reached adsorption saturation. Ultimately, **DTTB3** achieved an iodine vapor adsorption capacity of 4.60 g g^{-1}. Furthermore, it can be observed from the SEM image that the particle size of **DTTB3** after completing iodine vapor adsorption is larger than that of the original synthetic **DTTB3**, and its loose and porous structure is filled and covered with iodine (Fig. 2g). The EDS analysis and element mapping confirm that iodine has been successfully adsorbed onto **DTTB3**, exhibiting a uniform distribution throughout (Figures S2 and 2h-2k). Following the completion of desorption through methanol washing, a significant number of pore structures were restored on the polymer surface (Fig. 2l and m). By comparing the FT-IR and PXRD patterns of **DTTB3** before adsorption and after desorption iodine vapor, no obvious changes were detected, thereby confirming both strong stability and recyclability of **DTTB3** in industrial applications (Figs. S3 and S4).

3.3. Iodine adsorption in static aqueous solutions

Currently, numerous new materials have been reported to demonstrate exceptional performance in capturing gaseous iodine [41–43]. However, the iodine absorption capacity of these materials in aqueous media remains significantly inadequate. Previous research has indicated that **DTTB3** exhibits favorable adsorption properties for gaseous iodine. We further investigated its iodine absorption capabilities in aqueous

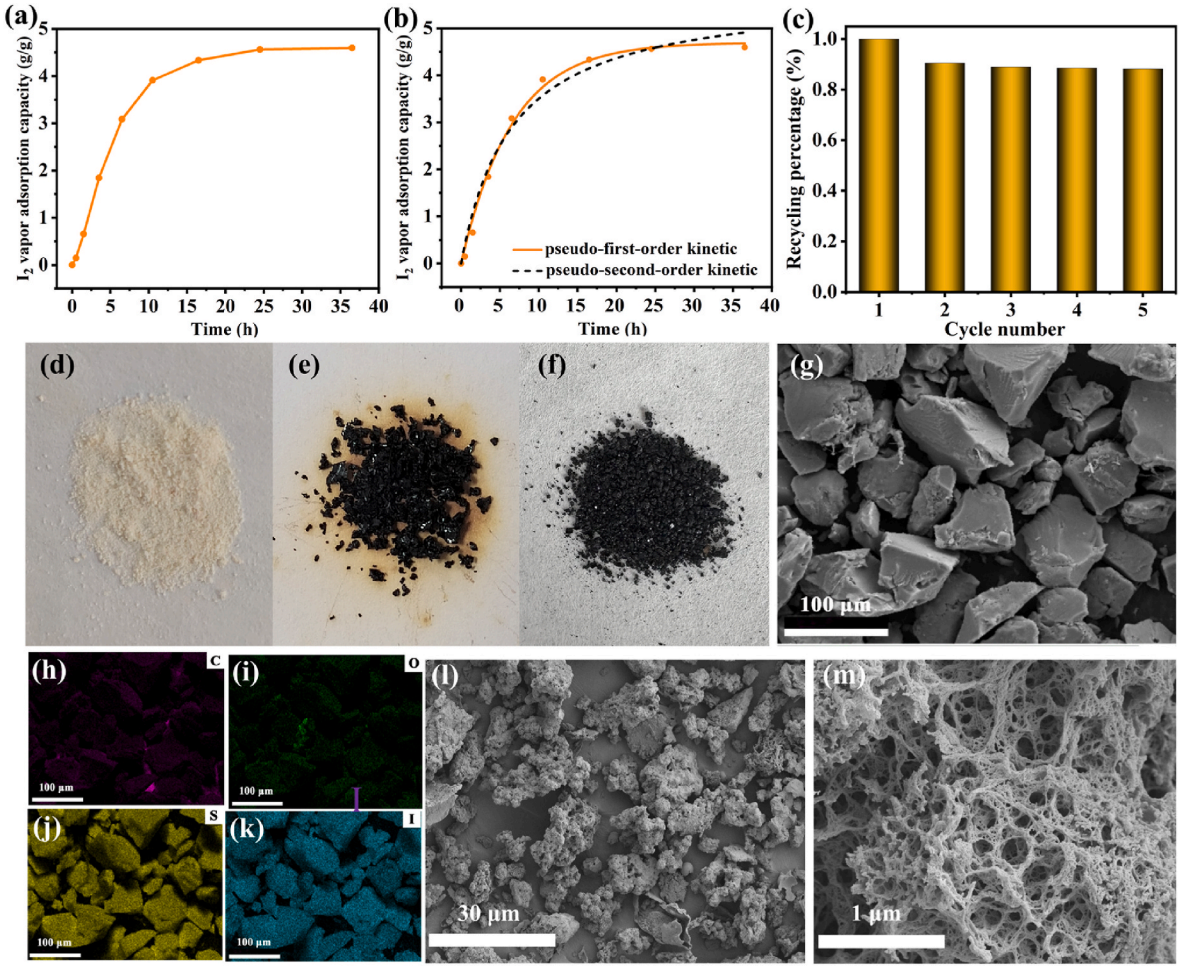

Fig. 2. Iodine vapor adsorption curve by **DTTB3** (a). The pseudo-first and pseudo-second order linear fitting plots for iodine vapor capture (b). Cyclic iodine vapor capture efficiency of **DTTB3** (b). Photos of **DTTB3** before adsorption (c), after adsorption (d) and desorption (e). SEM image of **DTTB3** after adsorbing iodine vapor (f). Elemental mapping graphs of **DTTB3** after adsorbing iodine vapor (g–j). SEM images of **DTTB3** after desorbing iodine vapor (k, l).

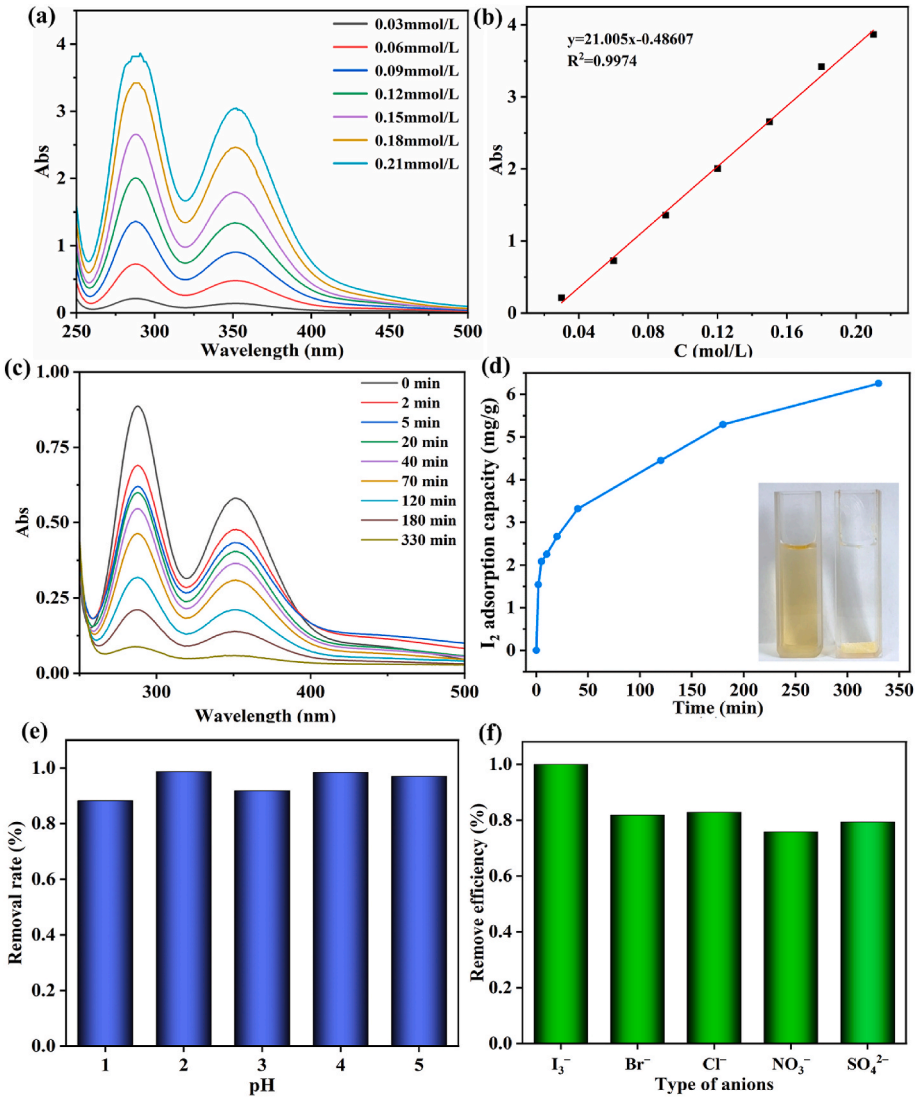

Fig. 3. (a) Absorbance variation curves of aqueous iodine solutions at different concentrations; (b) Linear fitting curve correlating absorbance with concentration for the standard aqueous iodine solution; (c) The curve of absorbance varying with time for a 0.12 mM aqueous iodine solution upon addition to **DTTB3**; (d) Efficiency of iodine adsorption by **DTTB3**; (e) Bar chart depicting removal efficiency of iodine from aqueous solutions with different pH values; (f) Bar chart showing removal efficiency of iodine from aqueous solutions containing interfering ions.

solutions. As illustrated in Fig. 3a, an increase in the concentration of the iodine solution corresponds with a concomitant rise in absorbance, indicating a positive correlation between absorbance (A) and concentration (C). The linear fitting curve representing the absorbance versus the concentration of standard aqueous iodine solutions is depicted in Fig. 3b. The relationship can be expressed by equation $A = 21.00\ C - 0.49$, with a linear correlation coefficient $R^2 = 0.9974$. It can be observed from Fig. 3c that upon the addition of 5 mg of **DTTB3** to a 0.12 mM iodine aqueous solution, the absorbance gradually decreased with the increase of time. After 2 min, the removal efficiency reached 22.20 % (Fig. 3c and d). When the same quantity of **DTTB3** was introduced into a 0.30 mM iodine aqueous solution for 3 min, the removal efficiency increased to 35.60 % (Fig. S5). As the reaction time extended, the absorbance continued to decline. After 330 min, both systems approached adsorption equilibrium, achieving removal efficiencies of 90.11 % and 95.15 %, with the maximum adsorption capacities were 6.25 and 24.58 mg g^{-1}, respectively. As illustrated in Fig. 3d, during the adsorption process, the color of the iodine solution changed from yellow to nearly colorless. Concurrently, the color of the adsorbent shifted from light yellow to yellow.

To assess the stability of **DTTB3**, FT-IR spectra and XRD patterns were analyzed before and after iodine adsorption from an aqueous solution. The FT-IR spectra revealed a significant reduction in the hydroxyl absorption peak within the range of 3300–3500 cm^{-1} (Fig. S6) [44]. This observation may be attributed to the interactions between iodine and the hydroxyl groups present in dithiothreitol components of **DTTB3** following adsorption, resulting in diminished hydroxyl signal intensity. In addition, the FT-IR spectrum of **DTTB3** after iodine desorption was also provided, which basically coincided with the spectrum of the original **DTTB3** (Fig. S7). Similarly, no significant changes were detected in PXRD patterns after iodine desorption (Fig. S8), suggesting that the crystalline structure of **DTTB3** remained largely intact throughout this process. Furthermore, it was confirmed that when the pH value of the aqueous solution ranged from 1 to 5, **DTTB3** exhibited a removal efficiency exceeding 88 % for a 0.12 mM iodine aqueous solution (Fig. 3e). This finding indicates that **DTTB3** can sustain high capacity for capturing iodine under various pH conditions. Additionally, **DTTB3** maintains decent iodine adsorption capacity even in high-concentration competing anion environments. As shown in Fig. 3f, Cl^-, Br^-, NO_3^-, and SO_4^{2-} interfered with iodine adsorption to different extents. The Cl^-, Br^-, and SO_4^{2-} caused minimal interference (adsorption capacity >80 %), while the NO_3^- leaded to increased interference, reducing **DTTB3**'s

iodine adsorption capacity to approximately 75 %.

3.4. Adsorption mechanism studies

In the X-ray photoelectron spectroscopy (XPS) spectrum of **I_2@DTTB3** (Fig. 4a), characteristic signals attributable to I_3^- were observed at binding energies of 629.6 and 618.1 eV, respectively. Concurrently, signals detected at 630.9 and 619.4 eV are indicative of the presence of I_5^- species [45]. The occurrence of I_3^- and I_5^- anions proves the adsorption of iodine by **DTTB3** in aqueous solution. The Raman spectrum serves as a powerful analytical tool for examining the state of I_2. The Raman spectra of **DTTB3**, both before and after iodine adsorption, are presented in Fig. 4b. It is evident that after the capture of iodine, two distinct peaks at 110 cm^{-1} and 165 cm^{-1} corresponding to **I_2@DTTB3** were observed. The peak at 110 cm^{-1} can be attributed to the symmetric stretching vibration of I_3^- anions, while the peak at 165 cm^{-1} is associated with the stretching vibration of polyiodide I_5^- [46]. Similarly, the XPS and Raman spectra of **DTTB3** adsorbing iodine vapor were also verified in a similar way. The I3d XPS spectrum of **DTTB3** demonstrated two binding energies at 631.0 and 618.8 eV, respectively (Fig. 4c). They correspond to the elemental iodine [47]. In Raman spectra, two distinct peaks at 110 cm^{-1} and 168 cm^{-1} corresponding to **I_2@DTTB3** were also appeared (Fig. 4d). The Raman spectra are clearly consistent with the XPS results, indicating strong interactions between the 3D organic polymers and iodine.

Density functional theory (DFT) calculations were performed to gain deeper insights into the adsorption mechanism. Firstly, the structure of **DTTB3** was optimized (Fig. 5a), and the electrostatic potential (ESP) diagram of its framework was computed (Fig. 5b). A high electrostatic potential region means that moving a positive charge to that region requires overcoming significant repulsive forces. On the contrary, the low electrostatic potential region means that it is easy to move a positive charge to this region, and the system energy will decrease. In order to gain a deeper understanding of the adsorption mechanism. Based on the results of electrostatic potential, select three regions of high, medium, and low electrostatic potential for comparison of adsorption energy. Through an analysis of DFT results in conjunction with previous studies [28,39,48,49], we deduced that the primary driving force for I_2/I_3^- absorption arises from various non-covalent interactions, including hydrogen bonds, I–I···π interactions, and electrostatic forces. The presence of $–CH_3$ and –OH groups, along with numerous benzene rings, facilitates the adsorption of I_2/I_3^- molecules via O–H···I (3.6826 and 2.6923 Å) bonds, C–H···I (3.1897, 3.7846, 3.3493, 3.2054, 3.7087, and 3.1112 Å) hydrogen bonds, I_2/I_3^-···π (3.4490 and 3.9455 Å) bonds as well as electrostatic interactions between I_2/I_3^- molecules and the polymer framework (Fig. 5c–h). Furthermore, by comparing the adsorption energies at different sites (Tables S1 and S2), it is evident that benzene rings exhibit the lowest adsorption energy for I_2/I_3^- molecules. This indicates that benzene rings within the polymer structure possess a superior capacity for I_2/I_3^- adsorption. In addition to the interactions outlined above, the polymer's high pore volume and extensive pore size range provide sufficient spatial capacity for iodine molecules, thereby facilitating the encapsulation of adsorbed iodine within its intrinsic cavity structure. Such a structural attribute of the polymer plays an indispensable role in the remediation of nuclear waste gases and liquids.

4. Conclusions

In summary, a novel type of three-dimensional organic polymer, namely **DTTB3**, was synthesized through a substitution reaction utilizing dl-dithiothreitol and 2,4,6-tribromomethyltrimethylbenzene as raw materials. The findings indicate that the polymer exhibits a strong adsorption capacity for iodine vapor, with a maximum adsorption capacity reaching 4.60 g g^{-1}. Notably, **DTTB3** eluted after iodine vapor adsorption can be reused in subsequent cycles of adsorption, demonstrating **DTTB3** shows excellent reusability. Furthermore, **DTTB3** also displays remarkable adsorption capacities in iodine aqueous solution, and the maximum adsorption capacities for iodine in 0.12 mM and 0.30

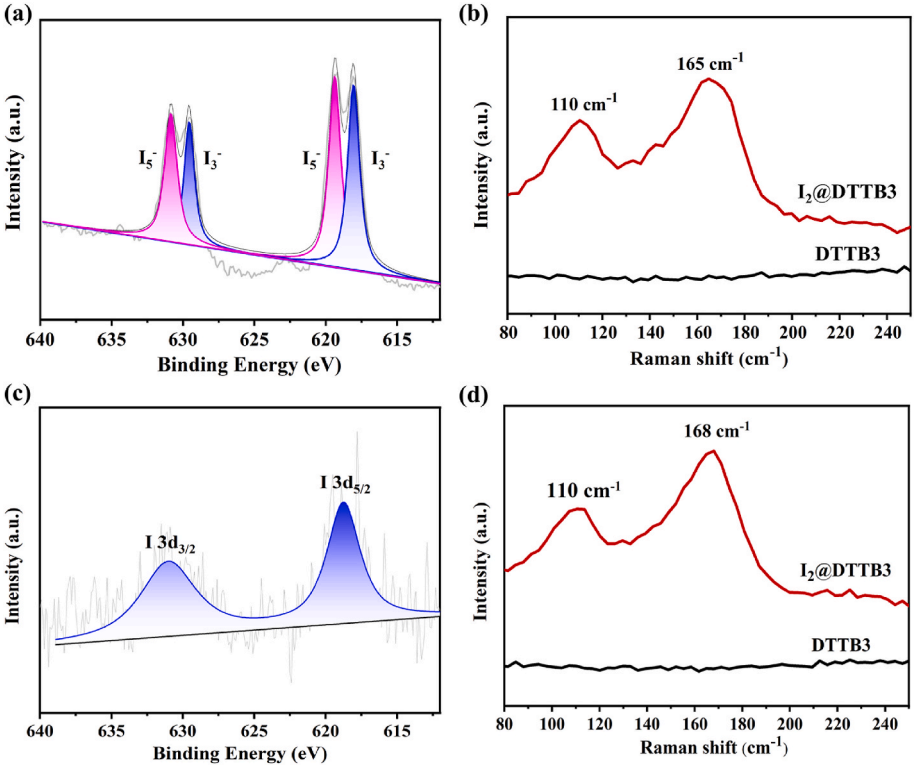

Fig. 4. XPS (a) and Raman spectra (b) of **I_2@DTTB3** for the adsorption of iodine in aqueous solution. XPS (c) and Raman spectra (d) of **I_2@DTTB3** for the adsorption of iodine vapor.

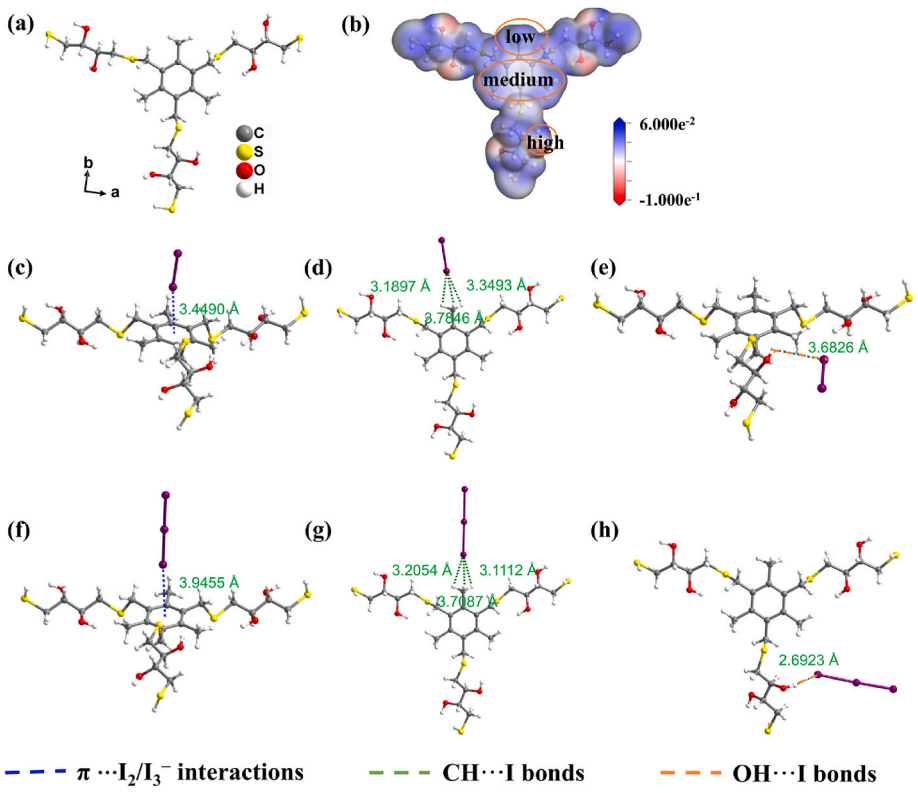

Fig. 5. The optimized computing model of **DTTB3** (a); The electrostatic potential map calculations of **DTTB3** (b); The adsorption interaction model between I_2 and benzene ring (c), $-CH_3$ (d) or $-OH$ (e); The adsorption interaction model between I_3^- and benzene ring (f), $-CH_3$ (g) or $-OH$ (h).

mM aqueous solutions were measured at 6.25 and 24.58 mg g^{-1}, respectively. Results from interference experiments reveal that the adsorption of iodine aqueous solutions under different pH conditions and interfering ions were no signification. These studies confirmed that **DTTB3** possesses highly efficient selectivity for iodine uptake. The organic polymer network developed in this study offers advantages such as straightforward preparation methods and low cost, thereby establishing a foundation for its application in large-scale water treatment processes. Concurrently, this work offers novel insights and viable avenues for addressing critical challenges associated with the recovery and reuse of iodine.

CRediT authorship contribution statement

Fei-Fei Wang: Writing – original draft, Investigation, Funding acquisition. **Qing-Rong Zhang:** Visualization, Data curation. **Chang Liu:** Writing – review & editing, Supervision. **Qian Zhang:** Resources, Conceptualization. **Guangyao Hou:** Visualization, Software. **Rui Zhang:** Writing – review & editing, Supervision.

Notes

The authors declare no competing financial interest.

Declaration of competing interest

The authors declare no competing financial interest.

Acknowledgments

This work was supported by the Fundamental Research Program of Shanxi Province (No. 202303021222230) and Natural Science Foundation of Liaoning Province (No. 2025-BS-0251).

Appendix A. Supplementary data

Supplementary data to this article can be found online at https://doi.org/10.1016/j.polymertesting.2025.109056.

Data availability

No data was used for the research described in the article.

References

[1] A.M. Rollo, A. Rollo, C. Mora, The tree-lined path to carbon neutrality, Nat. Rev. Earth Environ. 1 (7) (2020) 332, 332.
[2] L.G. Wang, D.S. Wang, Y.D. Li, Single-atom catalysis for carbon neutrality, Carbon Energy 4 (6) (2022) 1021–1079.
[3] G. Semieniuk, L. Taylor, A. Rezai, D.K. Foley, Plausible energy demand patterns in a growing global economy with climate policy, Nat. Clim. Change 11 (2021) 313–318.
[4] D. Dong, J.Y. Guan, Z.Q. Wang, Y.Q. Wang, Current status and trends of nuclear energy under carbon neutrality conditions in China, Energy 314 (2025) 134253.
[5] C. Wang, S.A. Raza, T.S. Adebayo, S. Yi, M.I. Shah, The roles of hydro, nuclear and biomass energy towards carbon neutrality target in China: a policy-based analysis, Energy 262 (2023) 125303.
[6] X.W. Liu, J.L. Liu, Y.K. Fan, G.Z. Xie, X.L. Sun, L.Y. Zhang, Q. Liu, X.Q. Yang, D. L. Duan, F.L. Qiao, C. Zhao, B.Z. Ge, S. Fang, S.H. Zhuang, W.D. Sun, Spatial-temporal variations of kelp ^{129}I contents in coastal waters of China before and after the Fukushima Daiichi Nuclear Power Plant accident, Mar. Pollut. Bull. 214 (2025) 117730.
[7] C.Y. Liu, H.Y. Wu, Y.Q. Wang, L.L. Li, J. Zhou, J.W. Wu, P. Lin, M.Y. Ni, Exploring the iodine adsorption and deposition behavior: an out-of-pile experiment on accident conditions of lead-bismuth fast reactor, J. Hazard. Mater. 495 (2025) 139116.
[8] S.Y. Sui, W. Lv, Y.H. Tian, Y.W. Wang, W. Xu, X.Y. Li, J.H. Li, Aluminum cluster molecular ring-based heterometallic framework materials for iodine capture, Ingor. Chem. 64 (2) (2025) 1146–1152.
[9] X. Gong, M.P. Short, T. Auger, E. Charalampopoulou, K. Lambrinou, Environmental degradation of structural materials in liquid lead-and lead-bismuth eutectic-cooled reactors, Prog. Mater. Sci. 126 (2022) 100920.
[10] H. Ding, M.C.D. Wilkins, C. Gausse, L.M. Mottram, S.K. Sun, M.C. Stennett, D. Grolimund, R. Tappero, S. Nicholas, N.C. Hyatt, C.L. Corkhill, Safely probing the

chemistry of Chernobyl nuclear fuel using micro-focus X-ray analysis, J. Mater. Chem. A 9 (21) (2021) 12612–12622.
[11] Y. Ma, J.J. Pan, H.Z. Rong, L. Liu, Y.L. Zhang, X.W. Cao, J.C. Zhang, T. Liu, N. Wang, Y.H. Yuan, Local charge density enhancement strategy in nitrogen-rich covalent organic framework for boosted iodine removal from water, Adv. Sci. 12 (30) (2025) e00697.
[12] W.A. Zhou, R. Lavendomme, D.W. Zhang, Recent progress in iodine capture by macrocycles and cages, Chem. Commun. 7 (2024) 779–792.
[13] C. Muhire, A.T. Reda, D.X. Zhang, X.Y. Xu, C. Cui, An overview on metal Oxide-based materials for iodine capture and storage, Chem. Eng. J. 431 (2022) 133816.
[14] X.H. Guan, Z.L. Shen, L. Chen, C. Zhang, C.G. Sun, Y. Du, B.C. Hu, C. Gao, A nitrogen-rich nanoporous ionic covalent organic framework as iodine adsorbent in gaseous and aqueous environments, ACS Appl. Nano Mater. 7 (23) (2024) 27318–27324.
[15] Z.Z. Zhang, L. Li, D. An, H.X. Li, X.H. Zhang, Triazine-based covalent organic polycalix[4]arenes for highly efficient and reversible iodine capture in water, J. Mater. Sci. 55 (4) (2020) 1854–1864.
[16] K. Baskaran, C. Elliott, M. Ali, J. Moon, J. Beland, D. Cohrs, S. Chong, B.J. Riley, D. Chidambaram, K. Carlson, Effects of NO_2 aging on bismuth nanoparticles and bismuth-loaded silica xerogels for iodine capture, J. Hazard. Mater. 446 (2023) 130644.
[17] W. Zheng, J.W. Huang, Z.Q. Tian, Z.Q. Yang, L.J. Leng, W.Z. He, J.F. Chen, X. Zeng, W.L. Yang, W.Q. Qu, H.L. Li, Metal sulfide functionalized activated carbon for efficient capture of gaseous iodine, Chem. Eng. Sci. 303 (2025) 120955.
[18] B.J. Riley, S.H. Chong, J. Schmid, J. Marcial, E.T. Nienhuis, M.K. Bera, S. Lee, N. L. Canfield, S. Kim, M.A. Derewinski, R.K. Motkuri, ACS Appl. Mater. Interfaces 14 (16) (2023) 18439–18452.
[19] J.F. Kurisingal, H. Yun, C.S. Hong, Porous organic materials for iodine adsorption, J. Hazard. Mater. 458 (2023) 131835.
[20] K. Kirakci, D. Buzek, P. Peer, V. Liska, J. Mosinger, I. Krízová, M. Kloda, S. Ondrusová, K. Lang, J. Demel, Polymeric membranes containing iodine-loaded UiO-66 nanoparticles as water-responsive antibacterial and antiviral surfaces, ACS Appl. Nano Mater. 5 (1) (2022) 1244–1251.
[21] Y. Yang, Y.M. Fu, Y.R. Tian, L. Zhao, C. Qin, X.L. Wang, Z.M. Su, Efficient iodine capture by metal-organic cubes based on hexanuclear vanadium clusters, Inorg. Chem. Front. 10 (21) (2023) 6221–6228.
[22] Z.L. Mo, D.Z. Tai, H. Zhang, A. Shahab, A comprehensive review on the adsorption of heavy metals by zeolite imidazole framework (ZIF-8) based nanocomposite in water, Chem. Eng. J. 443 (2023) 136320.
[23] Z.J. Li, Y. Ju, H.J. Lu, X.L. Wu, X.L. Yu, Y.X. Li, X.W. Wu, Z.H. Zhang, J. Lin, Y. Qian, M.Y. He, J.Q. Wang, Boosting the iodine adsorption and radioresistance of Th-UiO-66 MOFs via Aromatic substitution, Chem. Eur J. 27 (4) (2021) 1286–1291.
[24] X.R. Zhang, J. Maddock, T.M. Nenoff, M.A. Denecke, S.H. Yang, M. Schröder, Chem. Soc. Rev. 51 (8) (2022) 3243–3262.
[25] Y.H. Sun, S.A. Song, D.H. Xiao, L.F. Gan, Y.R. Wang, Easily constructed imine-bonded COFs for iodine capture at ambient temperature, ACS Omega 5 (38) (2020) 24262–24271.
[26] A. Karn, F. Sama, V.V. Chernyshev, J.N. Moorthy, An imidazole-integrated porous organic polymer as an expedient heterogeneous organocatalyst for one-pot synthesis of Pyrans, chromenes, and spiropyrans, ACS Appl. Polym. Mater. 7 (14) (2025) 9120–9130.
[27] A. Alsbaiee, B.J. Smith, L.L. Xiao, Y.H. Ling, D.E. Helbling, W.R. Dichtel, Nature 529 (2016) 190–194.
[28] J.J. Cao, H.T.Z. Zhu, L.Q. Shangguan, Y.Z. Liu, P.R. Liu, Q. Li, Y.T. Wu, F.H. Huang, A pillar[5]arene-based 3D polymer network for efficient iodine capture in aqueous solution, Polym. Chem. 12 (24) (2021) 3517–3521.
[29] J. Wang, L.L. Shen, L.L. Cai, H.Y. Li, Y.H. Zhang, Z.Y. Zhang, H. Zhang, F. Yu, Y. Q. Wang, Z.X. Li, Recyclable β-CD-crosslinked porous polymer networks for iodine capture, J. Mol. Struct. 1318 (2024) 139427.
[30] D. Xue, H.B. Zou, Y.P. Qiu, W. Lv, M.D. Madden, M.M. Xu, X.Y. Lian, C. Pulliam, E. A. Older, L.K. Hou, A. Campbell, T. de Rond, T. Awakawa, C.H. Yuan, B.S. Moore, J. Li, Discovery of acylsulfenic acid-featuring natural product sulfenicin and characterization of its biosynthesis, Nat. Chem. 17 (2025) 1011–1019.
[31] C. Liu, H.Y. Du, C. Xin, X. Di, Synthesis of porphyrin-based metal-organic framework and biomass-derived carbon composite for electrochemical detection of Rutin, J. Electroanal. Chem. 984 (2025) 119058.
[32] S. Mallick, S. Rana, K. Parida, A facile method for the synthesis of copper modified amine-functionalized mesoporous zirconia and its catalytic evaluation in C-S coupling reaction, Dalton Trans. 40 (36) (2011) 9169–9175.
[33] A. Ren, L. Qiao, K. Li, D. Zhu, Y. Zhang, Mitochondria-Targeted NIR ratiometric and colorimetric fluorescent probe for biothiols based on a thiol-chromene click reaction, Anal. Chem. 96 (2024) 17773–17780.
[34] Y.-X. Dong, C.-B. Li, M.-L. Jin, Z.-H. Gao, S. Ye, C_{Ar}−Br bond cleavage *via* cooperative EnT/NHC catalysis: mild access to indolines, Sci. China Chem. 67 (2024) 922–927.
[35] S. Sheshmani, M. Mardali, Harnessing the synergistic potential of ZnS nanoparticle-interfacing chitosan for enhanced photocatalytic degradation in aqueous media and textile wastewater, J. Polym. Environ. 32 (2024) 5783–5805.
[36] M.K. Ahmed, A.E. Shalan, M. Afifi, M.M. El-Desoky, S. Lanceros-Méndez, Correction to "Silver-Doped Cadmium Selenide/Graphene Oxide-Filled Cellulose Acetate Nanocomposites for Photocatalytic Degradation of Malachite Green toward Wastewater Treatment", ACS Omega 7 (21) (2022) 18190–18191.
[37] A. Phetrungnapha, N. Wiengnak, K. Maikrang, A low-cost water hyacinth-based adsorbent for free fatty acids removal from waste cooking oil: kinetic, isotherm, and thermodynamic studies, Braz. J. Chem. Eng. 42 (2025) 727–740.
[38] Z.H. Tian, W. Wei, S.W. Zhou, D.A. Wood, J.C. Cai, Experimental and fractal characterization of the microstructure of shales from sichuan basin, China, Energy Fuel. 35 (5) (2021) 3899–3914.
[39] Z. Jin, H. Yan, J. Zhu, Y. Xiao, C. Ni, Y. Luo, C. Liu, Y. Qin, J. Zou, Hypercross-linked polymers based on pillar[5]arene for highly efficient iodine adsorption, Chem. Eng. J. 522 (2025) 167939.
[40] J. Zhao, X. Yan, Z. Zhu, F. Li, S. Li, X. Liu, L. Li, J. Yang, Y. Hao, T. Chang, Linker-induced morphology of urea-functionalized ionic polymers for carbon dioxide immobilization and iodine separation, Sep. Purif. Technol. 374 (2025) 133643.
[41] B.Q. Wu, R.Z. Tang, Y. Liu, Z.W. Li, F. Lin, Z.Y. Sun, Y.Z. Pi, G.F. Ouyang, Y. Tan, Efficient iodine adsorption from seawater by simple macrocycle and mechanistic insights, Sci. China Chem. (2025), https://doi.org/10.1007/s11426-025-2668-9.
[42] Q.Q. Mao, S.Y. Yang, J.J. Zhang, Y.H. Liu, M. Liu, Post-synthetic modification of porous organic cages for enhanced iodine adsorption performance, Adv. Sci. 11 (45) (2024) 2408494.
[43] X.Y. Cao, Y.C. Jin, H.L. Wang, X. Ding, X.L. Liu, B.Q. Yu, X.N. Zhan, J.Z. Jiang, A tetraaldehyde-derived porous organic cage and covalent organic frameworks: syntheses, structures, and iodine vapor capture, Chin. Chem. Lett. 35 (9) (2024) 109201.
[44] N. Sun, Z.F. Meng, L.M. Zhen, Q.Y. Qin, W.H. Liu, J.B. Xue, Y.N. Sun, P. Tong, Effect of GO on oxytetracycline and Cu^{2+} co-adsorption in a yellow-brown soil, Appl. Surf. Sci. 702 (2025) 163345.
[45] W. Zhou, A. Li, M. Zhou, Y. Xu, Y. Zhang, Q. He, Nonporous amorphous superadsorbents for highly effective and selective adsorption of iodine in water, Nat. Commun. 14 (2023) 5388.
[46] R. Liu, Z. Wen, B. Zheng, J. Yang, M. Wang, X. Ding, L. Shi, H. Hu, T. Chen, S. Xiao, Y. Gao, Targeted design of three-dimensional covalent organic frameworks with full exposure of functional adsorption sites for efficient iodine capture, Sep. Purif. Technol. 370 (2025) 133234.
[47] W.-Y. Pei, J. Yang, H. Wu, W. Zhou, Y.-W. Yang, J.-F. Ma, A calix[4]resorcinarene-based giant coordination cage: controlled assembly and iodine uptake, Chem. Commun. 56 (2020) 2491–2494.
[48] F.F. Wang, B.S. Hou, Construction of zirconium/hafnium-oxo clusters based on a new protection-calix[8]arene, Dalton Trans. 53 (2024) 6507.
[49] L.J. Feng, J. Zhang, J.C. Zhang, X.W. Cao, Z.H. Guo, Y.H. Yuan, N. Wang, Supramolecular Organic Framework with Multidimensional Storage Spaces for Ultrahigh-Capacity Iodine Capture from Seawater vol. 8, Research, 2025, p. 608.